

Modeling and optimizations of triple-pass TDFAs for next-generation fiber optical communication systems

A. DINCER*, M. YÜCEL

Gazi University, 06560, Ankara, Turkey

The main goal of designing a multi-stage fiber amplifier is to achieve higher performance for long-haul optical transmission systems. In this paper, multi-stage triple-pass (TP) TDFAs are represented. Three types of TP-TDFA are modeled, optimized, and compared. Firstly, signal power, pump power, fiber length, and ion concentration were optimized in the input signal at the 1469 nm wavelength, which gives the highest gain in the S-band. Secondly, the input signals in the 1444-1499 nm band gap were amplified using these optimized values in all designs. Finally, all types were compared to conclude the best TP-TDFA.

(Received October 28, 2023; accepted June 3, 2024)

Keywords: Thulium-doped fiber amplifier (TDFA), Multi-stage, Triple-pass, Optimization

1. Introduction

Communication traffic has grown tremendously in recent years with high bandwidth applications such as video conferencing, online gaming, social networks, high-definition video streaming, and voice-over IP. While these new-generation technologies, the usage of which is increasing, require an increase in transmission speed and capacity, they also necessitate a change in the communication infrastructure. Fiber optic communication systems and optical amplifiers have a great share in meeting all these requirements [2-5]. The studies carried out to date are on Erbium Doped Fiber Amplifier (EDFA) with high efficiency in the C and L bands [6-10]. Since C and L bands may be insufficient, optical amplifiers that can operate effectively in the S-band are researched. Thulium Doped Fiber Amplifier (TDFA) and Fiber Raman Amplifier (FRA) are optical amplifiers with high efficiency in the S-band [11]. Due to some limitations of FRA, such as high pump power and multi-pump usage, TDFAs are seen as a better alternative. [12-14]. To increase the gain of TDFA, in some studies, the amplifier parameters were changed [15-20], while in others, different pumping configurations were tried to excite all Thulium ions [21-26]. In addition, in some research, the gain has been increased by adding a mirror or an optical circulator to the basic TDFA design with double-pass configurations [27-31]. In some, these designs are called double-pass; in others, they are called double-stage [30-31].

Multi-stage fiber amplifiers have fundamentally changed the architecture of long-haul optical communication systems and networks. Although studies of multi-pass optical amplifiers are mostly focused on double-pass, there are also studies of triple-pass (two-stage triple-pass and three-stage triple-pass) EDFA [32-34].

Akhter and Ibrahimy modeled all possible EDFA configurations, examined their characteristics, and compared them with each other [32,33]. In their study, S.W. Harun et al. used and compared two types of two-stage triple-pass EDFA [34]. On the other hand, considering the S-band, no study has been done on the TP-TDFA other than the research we have done before [30].

In this paper, multi-stage TP-TDFA structures are used, optimized, and compared for the next-generation fiber optical communication systems. There are three types of TP-TDFAs. The performance of each structure was analyzed using signal power, pump power, TDF length, and thulium ion concentration. All these parameters have been optimized, and the results have been examined. At the end of the study, all types were compared to determine the best TP-TDFA.

2. TP-TDFA designs

2.1. Simulation setups

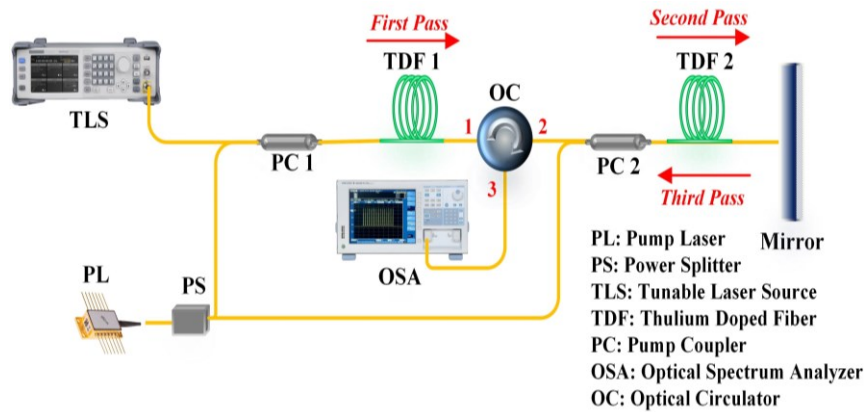
All types of TP-TDFA designs are respectively shown in Fig. 1, and simulated via OptiSystem 21.0. The first type, composed of one-stage single-pass TDFA and one-stage double-pass TDFA, is connected serially to obtain TP-TDFA. Fig. 1 (a) shows the schematic diagram of Type 1 TP-TDFA. The output signal of the first TDFA is the input signal for the second TDFA. In addition to TDFs, two pump couplers (PC), an optical circulator (OC), a power splitter (PS), and a mirror are used in Type 1 and Type 2 TP-TDFA designs. A PC combines the pump laser signal and input signal into the TDF. A circulator (CIR) is used to ensure the separation between the input and the output signal. A PS splits the power from two or more ports, and a mirror repasses the amplified signal through

the TDF.

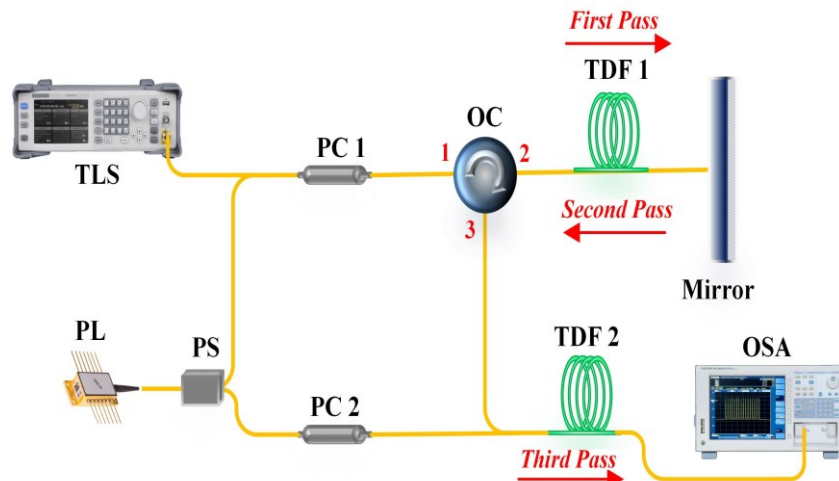
Type 2 TP-TDFA has a single pass TDF and a double pass TDF, as in Type 1. Differently, in Type 2, the signal first goes through the double pass TDF and then the single pass TDF. As a result, the output signal power of the double-pass TDF is the input signal power of the single-pass TDF, as shown in Fig. 1 (b). As in Type 1, in this setup, the pump power is divided into two by PS.

Fig. 1 (c) shows the Type 3 TP-TDFA design. It

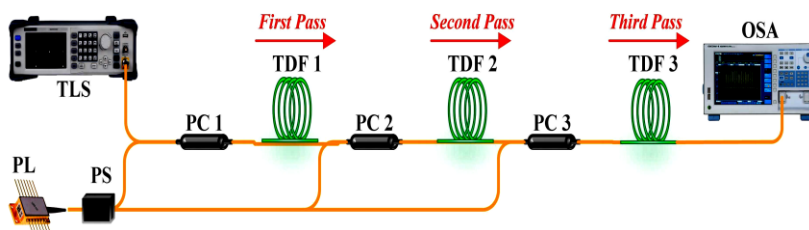
consists of a serial combination of three single-pass TDFs. The output signal power of the first TDF is the input signal power of the second thulium-doped fiber (TDF). The output signal power of the second TDF is the input signal power of the third TDF. Since the total signal passing through the TDFs is amplified three times, it is called TP-TDFA. Unlike the others in this setup, the pump power is divided into three by PS.



(a) Type 1



(b) Type 2



(c) Type 3

Fig. 1. TP-TDFA designs (color online)

2.2. Optimization steps

The cases to be tried in this study are listed in Table 1. In the first case, each design is simulated separately by feeding at different input power changed from -40 to 0 dBm, and the most efficient input power is determined.

In the second case, using the input power determined in the first case, each design is separately simulated by increasing 250 mW each time at pump powers between 250 and 3500 mW. Gain and noise figure spectra are created using the obtained values, and the most efficient pump power is determined.

Table 1. Input powers, pump powers, TDF lengths, and TDF ion concentration of all designs used in the simulations

	Input Power (dBm)	Pump Power (mW)	TDF Length (m)	TDF Ion Concent. (m^{-3})
Case 1	Between (-40) - 0	1000	5 (each TDF)	20e^{+24}
Case 2	The result of Case 1	Between 250 - 3500	5 (each TDF)	20e^{+24}
Case 3	The result of Case 1	The result of Case 2	Between 3 - 7	20e^{+24}
Case 4	The result of Case 1	The result of Case 2	The result of Case 3	Between 5e^{+24} - 30e^{+24}
Case 5	The result of Case 1	The result of Case 2	The result of Case 3	The result of Case 4

In case 3, using the values determined in the first and second cases, the TDF 1 length of Type 1 and Type 2 are optimized separately. Then, using the optimum TDF 1 length, the TDF 2 length has been simulated by the increment of 0.5 m each time between 3 and 7 m. Gain and noise figure spectra are created using the obtained values, and the most efficient TDF 2 length is determined. Then again, using the values determined in the first and second cases, the TDF 1 length of Type 3 is optimized. It is simulated using the optimum TDF 1 length by increasing 0.5 m each time at TDF 2 length between 3 and 7 m. After that, the most efficient TDF 2 length is determined. Then, using the optimum TDF 1 and TDF 2 lengths, it is simulated by increasing 0.5 m each time at the TDF 3 length between 3 and 7 m. Finally, gain and noise figure spectra are generated using the obtained values, and the most efficient TDF 3 length is determined.

In case 4, the ion concentrations of TDF 1, TDF 2, and TDF 3 are called ion concentration 1, ion concentration 2, and ion concentration 3, respectively. Using the values determined in the first, second, and third cases, the ion concentration 1 of Type 1 and Type 2 are optimized separately. Then, using the optimum ion

concentration 1, Type 1 and Type 2 were simulated by increasing $2.5\text{e}^{+24} \text{ m}^{-3}$ each time at ion concentration 2 between 5e^{+24} and $30\text{e}^{+24} \text{ m}^{-3}$. Gain and noise figure spectra of the ion concentration 2 are produced, and the optimum value is determined. Then again, using the values determined in the first, second, and third cases, ion concentration 1 of Type 3 is optimized. Secondly, the optimum ion concentration 1 is simulated by increasing $5\text{e}^{+24} \text{ m}^{-3}$ each time at ion concentration 2 between 5e^{+24} and $30\text{e}^{+24} \text{ m}^{-3}$. After that, the most efficient ion concentration 2 is determined. Then, using the optimum ion concentrations 1 and 2, it is simulated by increasing $5\text{e}^{+24} \text{ m}^{-3}$ each time at the ion concentration 3 between 5e^{+24} and $30\text{e}^{+24} \text{ m}^{-3}$. Finally, gain and noise figure spectra are generated using the obtained values, and the optimum ion concentration 3 is determined.

In the last case, using all values determined in the previous cases, all designs are simulated, and gain and noise figure spectra are produced using the obtained values in S bands. The parameters used in all simulations are listed in Table 2, and T_m emission cross-section spectra are shown in Fig. 2. Optisystem 21.0 uses the theoretical analysis of TDFAs in [35] for its calculations.

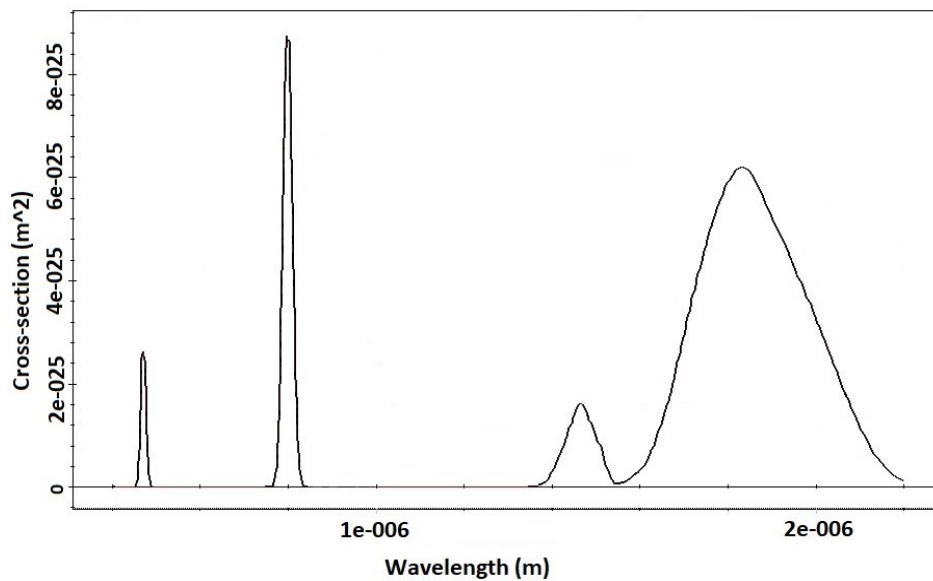
Fig. 2. T_m emission cross-section spectra used in the simulation

Table 2. Parameters used in the simulation

Parameter	Value	Unit
Core Radius	1.3	μm
Doping Radius	0.8	μm
Non-radiant ion lifetime 1	430×10^{-6}	s
Non-radiant ion lifetime 2	45×10^{-6}	s
Non-radiant ion lifetime 3	784×10^{-6}	s
Ar10	285.7	(1/s)
Ar30	1353.85	(1/s)
Ar31	138.46	(1/s)
The loss effects of PC	0.2	dB
The loss of PS	0.2	dB
The insertion loss of OC	0.2	dB
(K3101) Cross-relaxation coefficient	$0.18 e^{-21}$	m^{-3}/s
(K1310) Up-conversion coefficient	$5.12 e^{-24}$	m^{-3}/s

3. Simulation results

Gain and noise figure values were obtained by simulating all TP-TDFA designs separately. For easy comparison, these values were shown in two separate graphs as gain and noise figures.

In the first case, the input signal at 1469 nm wavelength, pumps at 1050 nm wavelength with 1000 mW power, 5 m length, and $20e^{+24}$ ion concentration for each TDF were applied to all designs. Each design was simulated separately by feeding at different input power changed from 0 dBm to -40 dBm. Fig. 3a shows the gain spectrum according to the input power, and Fig. 3b shows the spectrum of the noise figure according to the input power. According to Fig. 3a, -30 dBm was determined as the most efficient input power. While the noise figure values of Type 1 and 2 are close to each other, Type 3 is half of the others.

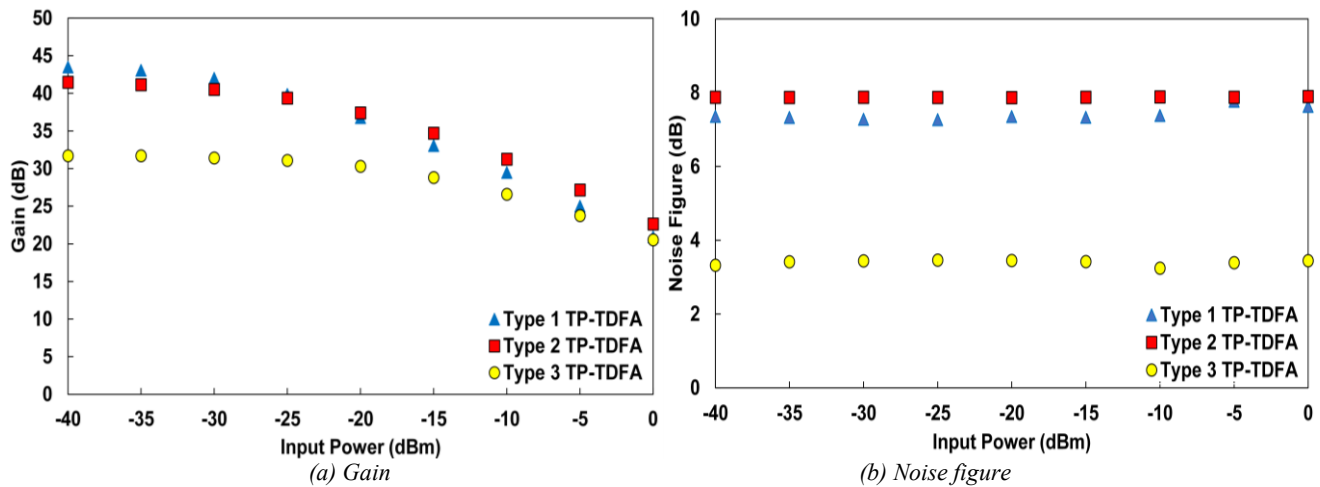


Fig. 3. Gain and noise figure graphs of all types of TP-TDFA fed at different input powers (color online)

In the second case, using -30 dBm, determined in the first case, each design was separately simulated by increasing 250 mW each time at pump powers between 250 and 3500 mW. Fig. 4 (a) shows the spectrum of the gain according to the wavelength, and Fig. 4 (b) shows the spectrum of the noise figure according to the wavelength.

It can be seen in Fig. 4 (a) that the most efficient pump power was 1750 mW for Type 1 and 2, while it was 2750 mW for Type 3. When the noise figure spectra in Fig. 4 (b) are considered, it is seen that the noise figures of Type 2 are higher. This increase is attributed to the higher counter-propagating ASE at the input part of the amplifier.

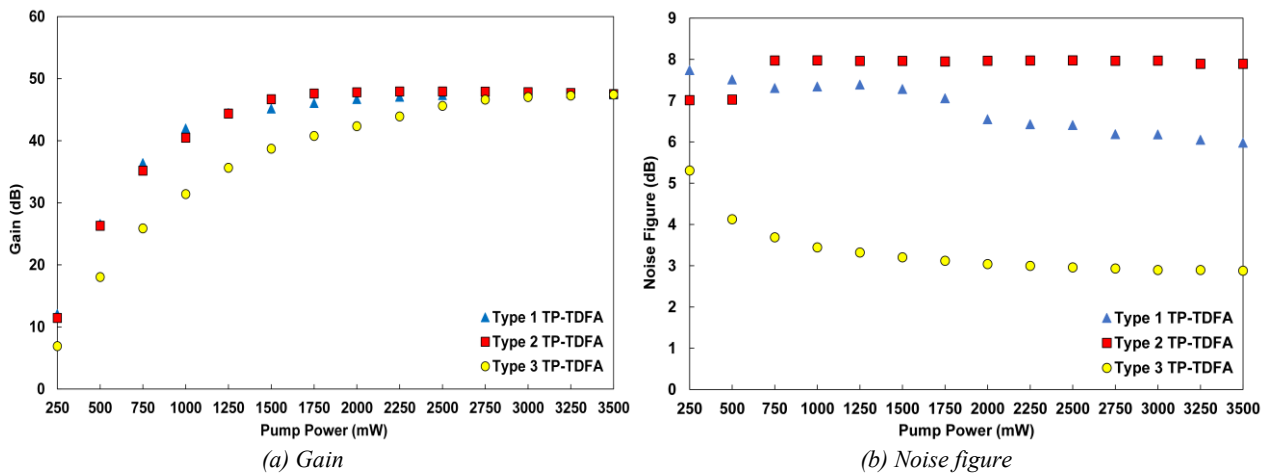


Fig. 4. Gain and noise figure graphs of all types of TP-TDFA fed at different pump powers (color online)

In case 3, using 1750 mW, which was determined as the optimum pump power for Type 1 and Type 2 in the second case, TDF 1 of Type 1 and Type 2 were optimized separately using the software, which was 5.2 m for both of them. Then, using TDF 1: 5.2 m, Type 1 and Type 2 were simulated by increasing 0.5 m each time at TDF 2 length between 3 and 7 m. Fig. 5a shows the spectrum of the gain according to the TDF 2 length, and Fig. 5b shows the

spectrum of the noise figure according to the TDF 2 length. In Fig. 5 (a), it can be seen that the optimum value of TDF 2 length for Type 1 is 5.5 m, and the optimum value of TDF 2 for Type 2 is 5 m. These values continued to be used in the next case. In Fig. 5 (b), it is seen that the noise figure values of these types are close to each other.

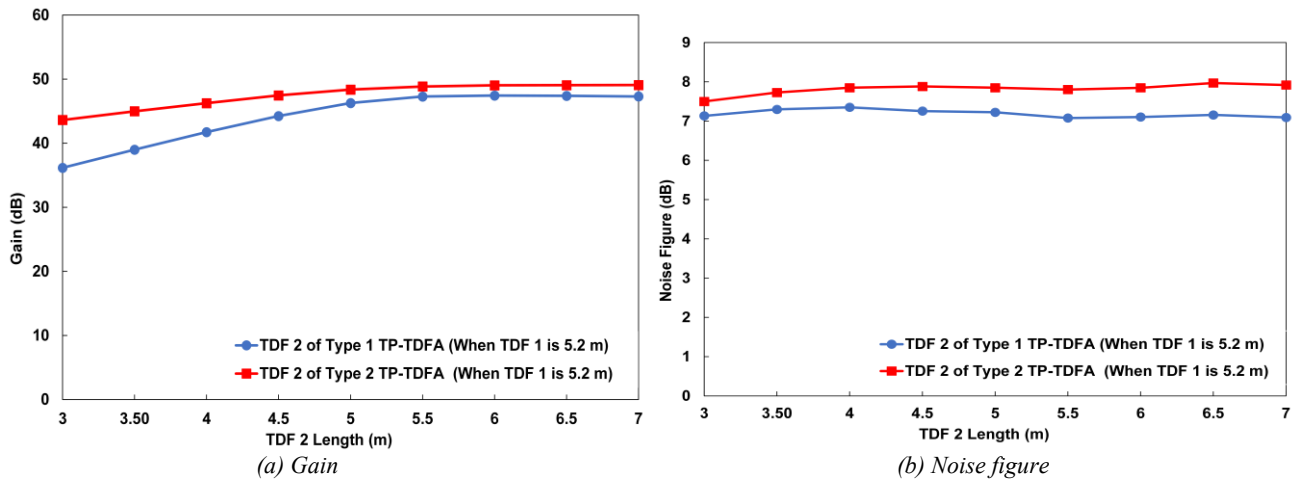


Fig. 5. While optimum TDF 1 is 5.2 m, TDF 2 lengths versus gain and noise figure of Type 1 & Type 2 of TP-TDFA (color online)

Then again, using 2750 mW, determined as the optimum pump power for Type 3 in the second case, TDF 1 of Type 3 was optimized using the software, and it was 6.3 m. It was simulated by increasing 0.5 m each time at TDF 2 length between 3 and 7 m while using TDF 1: 6.3 m constant. Fig. 6a shows the spectrum of the gain according to the TDF length, and Figure 6b shows the spectrum of the noise figure according to the TDF length.

As shown in Fig. 6a, the most efficient TDF 2 length is 6 m. Then, using the optimum TDF 1: 6.3 m and TDF 2: 6 m lengths, it was simulated by increasing 0.5 m each time at TDF 3 length between 3 and 7 m. Finally, the obtained values were added in Fig. 6. The most efficient TDF 3 length is 3.5 m. The noise figure values are lower since the third TDF is near saturation.

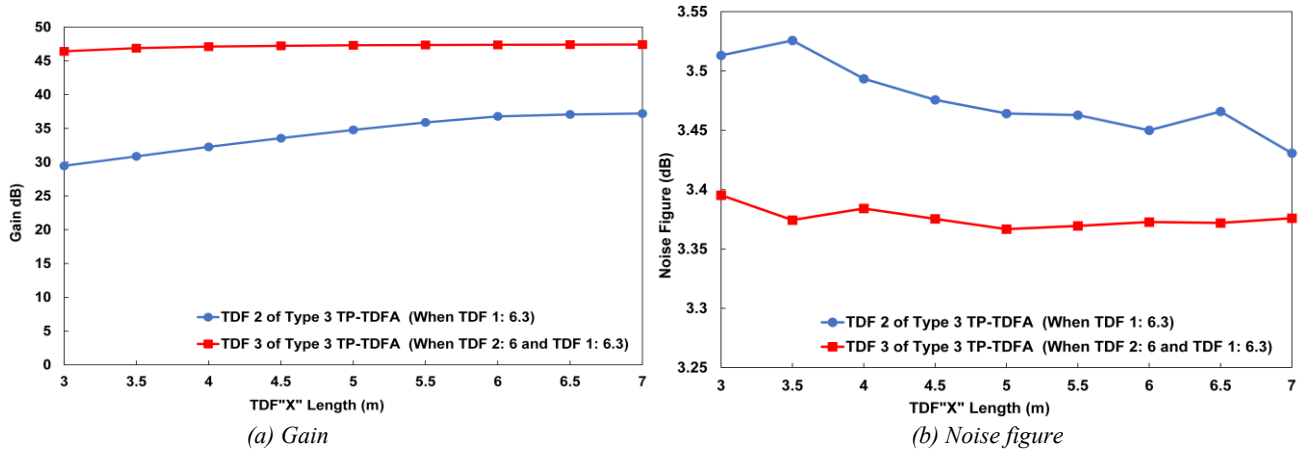


Fig. 6. Gain and noise figure graphs of Type 3 TP-TDFA with different TDF lengths (color online)

In case 4, using TDF 1: 5.2 m and TDF 2: 5.5 m, which were determined the optimum lengths for Type 1 and Type 2 in the third case, ion concentration 1 of Type 1 and Type 2 were optimized separately, and it was $18e^{+24} m^{-3}$ for both of them. Then, using ion concentration 1: $18e^{+24} m^{-3}$, Type 1 and Type 2 were simulated by increasing $2.5e^{+24} m^{-3}$ each time at ion concentration 2

between $5e^{+24}$ and $30e^{+24} m^{-3}$. Fig. 7 (a) and (b) shows the gain spectrums and the noise figure according to ion concentration 2. Fig. 7 (a) shows that $20e^{+24} m^{-3}$ is the optimum value of ion concentration 2 for Type 1, and $22.5e^{+24} m^{-3}$ is the optimum value of ion concentration 2 for Type 2. These values continued to be used in the next case.

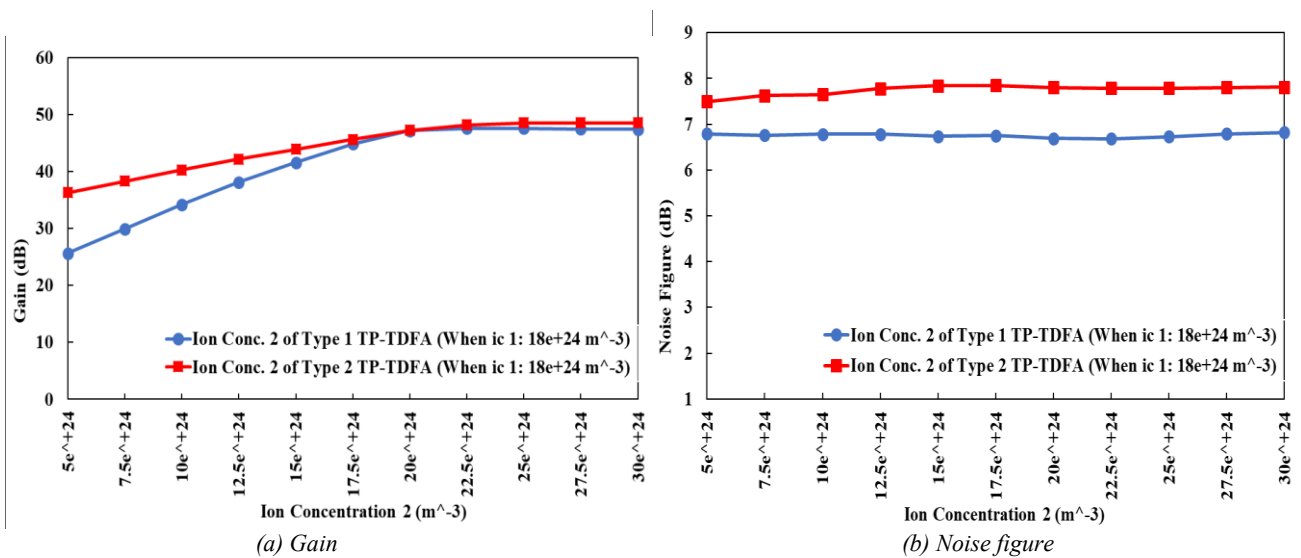


Fig. 7. While optimum ion concentration 1 is $18e^{+24}$, ion concentration 2 versus gain and noise figure of Type 1 & Type 2 of TP-TDFA (color online)

Then again, using TDF1: 6.3 m, TDF 2: 6 m, and TDF 3: 3.5 m, which was determined the optimum TDF lengths for Type 3 in the third case, ion concentration 1 of Type 3 was optimized by using the software, and it was $16e^{+24} m^{-3}$. Using ion concentration 1: $16e^{+24} m^{-3}$, it was simulated by increasing $2.5e^{+24} m^{-3}$ each time at ion concentration 2 between $5e^{+24}$ and $30e^{+24} m^{-3}$. Gain and noise figure graphs in Fig. 8 were created using the obtained values. As shown in Fig. 8 (a), $22.5e^{+24} m^{-3}$ is the optimum value of ion concentration 2 for this type. Then,

the optimum ion concentration 1: $16e^{+24} m^{-3}$ and ion concentration 2: $22.5e^{+24} m^{-3}$ was simulated by increasing $2.5e^{+24} m^{-3}$ each time at ion concentration 3 between $5e^{+24}$ and $30e^{+24} m^{-3}$. Finally, the obtained values were added in Fig. 8. The most efficient ion concentration 3 is $17.5e^{+24} m^{-3}$. Additionally, since the third TDF is near saturation, the noise figure values are slightly lower. The noise figure is 3.45 dB at the $17.5e^{+24} m^{-3}$ ion concentration. When noise figures of other ion concentrations are considered, this value is average.

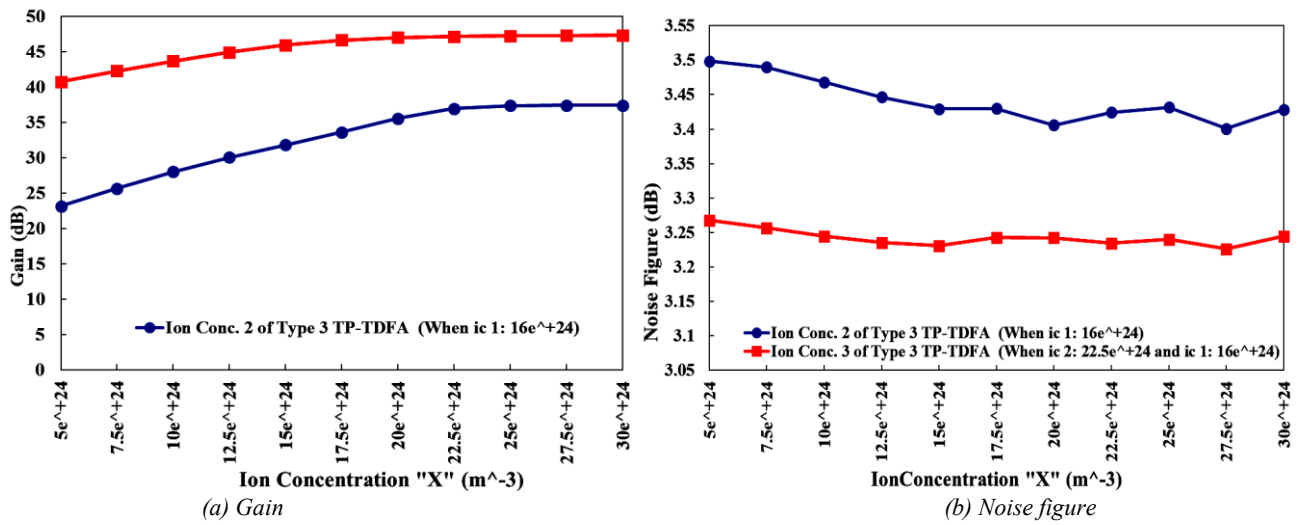


Fig. 8. Gain and noise figure graphs of Type 3 TP-TDFA with different ion concentrations (color online)

All optimization studies so far have been conducted on the input signal at 1469 nm wavelength, which is the highest gain obtained from the S-band. The values obtained for this signal listed in Table 3 were applied to the input signals in the 1444-1499 nm wavelength range

(S-band). The values of Type 1 and Type 2 are quite close. TDF 2 of Type 1 is slightly longer, while the ion concentration 2 of Type 2 is slightly higher. For easier comparison, the obtained gain and noise graphs of all types are shown in Fig. 9.

Table 3. Optimized values were determined in all cases

	Input Power (dBm)	Pump power (mW)	TDF Length (m)	TDF Ion Concentration (m ⁻³)
Type 1	(-30)	1750	TDF 1: 5.2, TDF 2: 5.5	ion conc. 1: 18e ⁺²⁴ , ion conc. 2: 20e ⁺²⁴
Type 2	(-30)	1750	TDF 1: 5.2, TDF 2: 5	ion conc. 1: 18e ⁺²⁴ , ion conc. 2: 22.5e ⁺²⁴
Type 3	(-30)	2750	TDF 1: 6.3, TDF 2: 6, TDF 3: 3.5	ion conc. 1: 16e ⁺²⁴ , ion conc. 2: 22.5e ⁺²⁴ , ion conc. 3: 17.5e ⁺²⁴

As shown in Fig. 9 (a), the gain values of the models optimized for the signal in the 1469 nm wavelength are 44.64 dB for Type 1, 45.67 dB for Type 2, and 43.95 dB for Type 3. While the highest gain and noise figure values belong to Type 2, the lowest gain and noise figure values

belong to Type 3. The gain values of Type 2 are higher than Type 1. As a result, the gain value of the signal amplified with a single pass after a double pass is higher than that of a double-pass amplified signal used after a single pass.

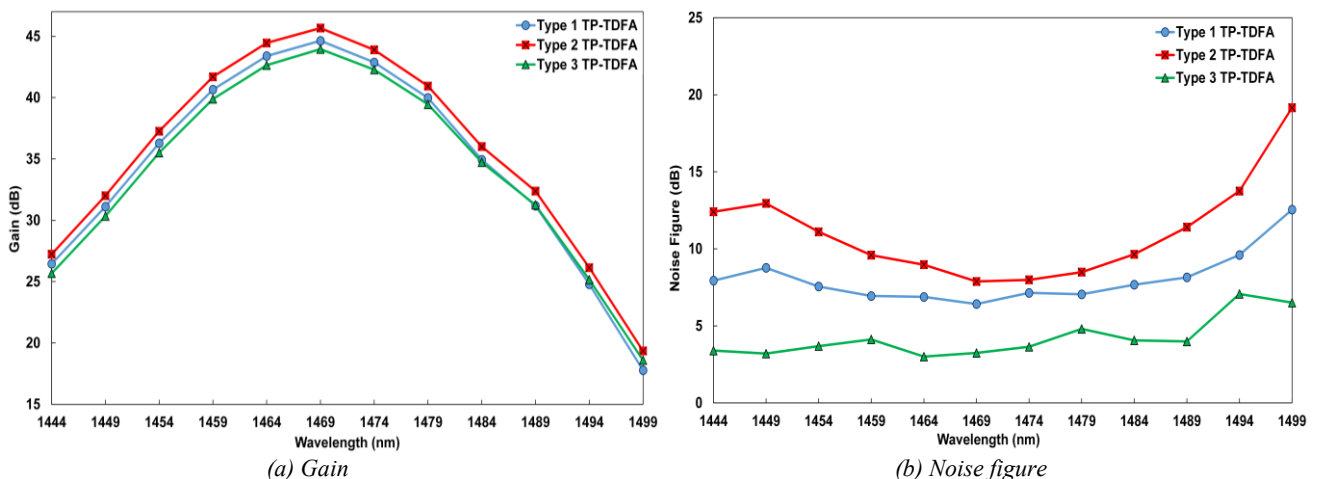


Fig. 9. Gain and noise figure graphs of all types of TP-TDFA at optimized values (color online)

The highest noise figure values have occurred in the Type-2 design. This increase is attributed to the higher counter-propagating ASE at the input part of the amplifier. This reduces the population inversion at the input part of TDF and afterward increases the noise figure [29].

4. Conclusion

Three types of TP-TDFA have been presented in this research. Input power, pump power, TDF length, and ion concentration were optimized for all three types, respectively. Then, the performance comparison was made over the gain and noise figure values in the S-band for all types using the determined optimized values. Examining the gain performance of all optimized TP-TDFA types, it can be concluded that Type 2 is the best design. Nevertheless, the noise figure values of designs are higher than other types and seem to be a disadvantage. On the other hand, considering the noise figure graphs in Fig. 9

(b), Type 3 has less than half of the noise figure values of the other types and seems to be the best choice for systems requiring low noise. If a comparison is made by looking at the results obtained, two-stage triple-pass models (Type 1 & 2) are more useful and economical than the three-stage triple-pass model (Type 3). Using these two types, whose gain values are high and close to each other, can increase the repeater distance in long-haul next-generation fiber optical communication systems.

A comparison of similar designs in the literature is made in Table 4. There are two TP-TDFA studies; our previous study [30] and another study close to the 2000 nm band [26]. Since no other studies have been found, a comparison has been made with TP-EDFA. Since different doped materials, input signal bandwidths, parameters, equipment, and techniques are used in different studies, gain and noise figures also differ. However, in general terms, similar gains were obtained from TP-EDFA designs and TP-TDFA designs.

Table 4. Comparison with similar design studies in the literature

Design	Input Power (dBm)	Signal Wavelength (nm)	Pump Power (mW)	Fiber Length (m)	Gain (dB)	Noise Figure (dB)
Type 1 TDFA (current study)	-30	1469	1750	5,2+5,5	44,6	6,4
Type 2 TDFA (current study)	-30	1469	1750	5,2+5	45,6	7,8
Type 3 TDFA (current study)	-30	1469	2750	6,3+6+3,5	43,9	3,3
Type 1 TDFA[26]	0	1975	200	3+4	19,9	~ 5,6
Type 1 TDFA[30]	-20	1469	1000+1000	5+4,8	~ 42,7	~ 10
Type 1 EDFA[32]	-20	1550	10+50	-	~ 55,0	~ 3,5
Type 1 EDFA[33]	-	-	150+240	-	78,7	3,3
Type 1 EDFA[34]	-20	1550	100	10	~ 42,0	~ 7,0
Type 1 EDFA[36]	-30	1560	300	6+11	54,9	3,7
Type 2 EDFA[32]	-20	1550	10+50	-	~ 35,0	~ 3,9
Type 2 EDFA[33]	-	-	150+240	-	59,6	8,1
Type 2 EDFA[34]	-20	1550	100	10	~ 41,0	~ 7,0
Type 2 EDFA[37]	-30	1550	30+70	10+7	~ 42,0	~ 5,4
Type 3 EDFA[32]	-20	1550	10+50+100	-	~ 40,0	~ 4,6
Type 3 EDFA[33]	-	-	150+240+290	-	58,5	7,0

References

- [1] D. Vargo, L. Zhu, B. Benwell, Z. Yan, Hum. Behav. Emerg. Tech. **3**, 13 (2021).
- [2] Y. Sun, A. K. Srivastava, J. Zhou, J. W. Sulhoff, Bell Syst. Tech. J. **4**(1), 187 (1999).
- [3] S. Singh, A. Singh, R. S. Kaler, Optik **124**(2), 95 (2013).
- [4] X. Ding, G. Wu, F. Zuo, J. Chen, Optoelectron. Lett. **15**(6), 401 (2019).
- [5] D. Malik, G. Kaushik, A. Wason, J. Opt. **47**(3), 396 (2018).
- [6] M. Yücel, H. H. Göktas, G. Akkaya, 2012 20th Signal Processing and Communication Applications, 1 (2012).
- [7] M. Yucel, Z. Aslan, Microw. Opt. Tech. Lett. **55**, 2525 (2013).
- [8] J. A. Bebawi, I. Kandas, M. A. El-Osairy, M. H. Aly, Appl. Sci. **8**(9), 1640 (2018).
- [9] N. M. Anwar, S. El-Sahn, E. El-Badawy, M. H. Aly, Opt. Quant. Electron. **52**, 109 (2020).

- [10] O. Akcesme, M. Yucel, M. Burunkaya, *Optik* **239**, 166850 (2021).
- [11] J. Kani, M. Jinno, *Electron. Let.* **35**(2), 1004 (1999).
- [12] S. Zhu, S. Pidishety, Y. Feng, S. Hong, J. Demas, R. Sidharthan, S. Yoo, S. Ramachandran, B. Srinivasan, J. Nilsson, *Opt. Express* **26**(18), 23295 (2018).
- [13] A. H. M. Husein, F. I. El-Nahal, *Optik* **124**(19), 4052 (2013).
- [14] Z. Li, A. M. Heidt, J. M. O. Daniel, Y. Jung, S. U. Alam, D. J. Richardson, *Opt. Express* **21**(8), 9289 (2013).
- [15] S. Aozasa, H. Masuda, M. Shimizu, *J. Lightwave Technol.* **24**(10), 3842 (2006).
- [16] F. I. El-Nahal, A. Hakeim, N. Husein, *Open J. Appl. Sci.* **2**(4), 5 (2012).
- [17] R. Singh, M. L. Singh, 2016 International Conference on Recent Advances and Innovations in Engineering, 1 (2016).
- [18] I. Kaur, N. Gupta, *Int. J. Comput. Digit. Syst.* **3**(3), 227 (2014).
- [19] K. P. W. Dissanayakel, S. D. Emami, H. A. Abdul-Rashidi, S. M. Aljamimi, Z. Yusoff, M. I. Zulkifli, S. Z. Muhamad-Yassin, K. A. Mat-Sharif, N. Tamchek, 2013 IEEE 4th International Conference on Photonics (ICP), 288 (2013).
- [20] M. Yücel, A. Dincer, *Duzce Uni. J. Sci. Tech.* **8**(3), 2062 (2020).
- [21] R. Singh, M. L. Singh, B. Kaur, *Optik* **123**(20), 1815 (2012).
- [22] S. H. Yam, Y. Akasaka, Y. Kubota, H. Inoue, K. Parameswaran, *IEEE Photon. Technol. Lett.* **17**(5), 1001 (2005).
- [23] F. Roy, D. Bayart, A. Sauze, P. Baniel, *IEEE Photon. Technol. Lett.* **13**(8), 788 (2001).
- [24] A. S. L. Gomes, M. T. Carvalho, M. L. Sundheimer, C. J. A. Bastos-Filho, J. F. Martins-Filho, M. B. Costa e Silva, J. P. von der Weid, W. Margulis *IEEE Photonics Technology Letters* **15**(2), 200 (2003).
- [25] R. Singh, M. L. Singh, *Optik* **140**, 565 (2017).
- [26] M. S. K. Jamalul, N. M. Yusoff, A. H. Sulaiman, *Indones. J. Electr. Eng. Comput. Sci.* **15**(3), 1203 (2019).
- [27] S. D. Emami, S. W. Harun, H. A. Abdul-Rashid, S. A. Daud, H. Ahmad, *Prog. Electromag. Res. B.* **14**, 431 (2009).
- [28] C. J. A. Bastos-Filho, J. F. Martins-Filho, The 2003 SBMO/IEEE MTT-S International Microwave and Optoelectronics Conference, 125 (2003).
- [29] S. D. Emami, S. W. Harun, H. A. Abdul-Rashid, S. A. Daud, H. Ahmad, F. Abd-Rahman, Z. A. Ghani, *Optik* **121**(4), 1257 (2010).
- [30] M. Yucel, A. Dincer, *Microw. Opt. Technol. Lett.* **64**(10), 1863 (2022).
- [31] D. Mohammed, A. Hammadi, *J. Opt. Commun.* **44**(1), 55 (2023).
- [32] F. Akhter, *Int. J. Phys. Sci.* **7**(18), 2656 (2012).
- [33] F. Akhter, A. W. Naji, M. I. Ibrahimy H. R. Siddiqui, 2012 International Conference on Computer and Communication Engineering (ICCCE), 462 (2012).
- [34] A. W. Naji, H. F. H. Ibrahim, B. Ahmed, S. W. Harun, M. A. Mahdi, International Conference on Computer and Communication Engineering (ICCCE'10), 1 (2010).
- [35] P. Peterka, B. Faure, W. Blanc, M. Karasek, B. Dussardier, *Optical and Quantum Electronics* **36**(1-3), 201 (2004).
- [36] S. Qin, J. He, Y. Zou, Z. Qiang, Asia Communications and Photonics Conference and Exhibition, Shanghai, 15 (2010).
- [37] K. A. Khairi, A.W. Naji, S. J. Sheih, M. A. Mahdi, *Microwave and Optical Technology Letters* **41**(4), 317 (2004).

*Corresponding author: ayten.dincer1@gazi.edu.tr